Sharp exponential band tails in highly disordered lead sulfide quantum dot arrays

Peter T. Erslev, Hsiang-Yu Chen, Jianbo Gao, Matthew C. Beard, Arthur J. Frank, Jao van de Lagemaat, Justin C. Johnson, and Joseph M. Luther

Phys. Rev. B **86**, 155313 — Published 17 October 2012

DOI: 10.1103/PhysRevB.86.155313

Sharp Exponential Band Tails in Highly Disordered Lead Sulfide Quantum Dot Arrays

Peter T. Erslev, Hsiang-Yu Chen, Jianbo Gao, Matthew C. Beard, Arthur J. Frank, Jao van de Lagemaat, Justin C. Johnson, and Joseph M. Luther

National Renewable Energy Laboratory, 15013 Denver West Parkway, Golden, Colorado 80401, USA

We employ temperature-dependent, illumination intensity modulated photocurrent spectroscopy (IMPS) to investigate the intra band gap density of states in films of PbS quantum dots (QDs). Using both co-planar electrode and stacked photovoltaic device configurations, IMPS measurements of PbS QD arrays show evidence for carrier trapping in exponential band tails extending from the band edges into the gap. The band tails have characteristic energies near 14 meV, similar to those found in other larger grain, polycrystalline bulk semiconductors rather than the large Urbach energies normally associated with nanocrystals and porous/polycrystalline films. This result helps explain recent success in using QD solids in device applications and indicates potential for QD materials to compete with bulk materials in semiconductor applications.

Colloidal quantum dot (QD) films, which maintain quantum-size effects from constituent particles and efficiently transport charge are scientifically and technologically of great interest [1-4]. Such QD films are used in place of bulk semiconductors to fabricate many optoelectronic devices (photovoltaics (PVs), photodetectors, light-emitting devices, etc). While the device performance may still be developing, the potential advantages are evident. Aside from increasing the bandgap of the semiconductor, quantum confinement can provide additional benefits such as efficient multiple exciton generation [5], enabling a path toward inexpensive yet efficient PVs [6, 7].

While the efficiency of QD solar cells is ever-improving [8, 9], the mechanism of exciton dissociation and subsequent charge-carrier transport within the QD array is under debate and likely depends on morphological and chemical attributes[10]. Researchers have reported nearest-neighbor, variable range hopping, [11, 12], and band-like transport characteristics[2, 13, 14]. Nagpal and Klimov concluded that conduction occurs primarily through a mid-gap band of states in the dark, while photogenerated charges move within the conduction or valence band [14].

Colloidal QDs are characterized by well-defined, defect-free single crystalline cores with large surface area to volume ratios. Long alkyl molecules that terminate QD-surfaces must be removed or replaced to promote QD-QD coupling. The process by which ligands are exchanged introduces disorder on micro- and macroscopic length scales. Ordered QD arrays that can exhibit coherent transport are a goal of many researchers, [15-17] but have yet to be achieved. Conductive films often show macroscopic cracks [18] as well as large orientational and positional disorder of the constituent QDs. Furthermore, as synthesized, PbS QDs possess an excess of surface Pb-atoms, which anchor the thiol moiety of molecules such as 1,2-ethanedithiol (EDT) and 3-mercaptopropionic acid which alters the stoichiometry of the QDs[19]. QDs are faceted and ligand molecules bind in various configurations on each surface [20]. Various techniques

have measured carrier densities of 10^{15}-10^{16} cm^{-3} [1, 9, 21] corresponding to a single ionized hole over ~100 QDs while each QD possesses nearly half as many bound surface ligands as the number of core atoms. On top of the ligand induced disorder, the best size distributions is on the order of 5% (corresponding to ~1 monolayer), but yields nearly a 100-meV discrepancy between low-energy electronic states. In spite of these hurdles, carrier transport can still be fairly efficient. PbS and PbSe QD solar cells have shown short-circuit carrier densities on the order of 30 mA/cm^2, with internal quantum efficiencies greater than 80% across the visible spectrum[6].

Liu *et al*. [22] measured the ligand-length dependence of both electron and hole mobilities of thiol-treated QD PbSe films. The effective mobility has an exponential dependence on the ligand length (or QD spacing), with mobility values ranging from 10^{-1} to 10^{-4} $cm^2V^{-1}s^{-1}$ as the ligand length increased from 4 Å to 9 Å [22], indicating weak electronic coupling. Surprisingly, there were no observable changes in the transport characteristics when the QD-size dispersion was varied, suggesting a dominant conduction pathway that is insensitive to variations in the $1S_e$ and $1S_h$ states of the QDs. This illustrates that the transport mechanism seems to strongly depend on the QD/surrounding composition and array processing conditions. Higher mobilities were found recently in QD arrays with *inorganic* ligands, on the order of 3-15 $cm^2V^{-1}s^{-1}$, suggesting mean free paths extending over several strongly-coupled QDs[2]. Earlier work on transport though silicon nanocrystal films invoke space-charge-limited or tunneling conduction with geometric and charging effects that alter conduction as well as the intrinsic properties of the nanocrystals [23].

QD films may appear most akin to disordered amorphous or polycrystalline solids due to porosity, randomized QD packing, high QD surface area, and non-stoichiometric [24] and/or other properties influenced by ligands [24]. In most disordered semiconductors transport kinetics are determined by an exponentially decreasing density of states (DOS) ($N(E)=N_0*exp(-\Delta E/E_U)$, where $\Delta E = E_C-E$ or $\Delta E = E-E_V$ and E_U is a characteristic energy describing the exponential distribution) from the edge of the conduction or valence band edge also known as the Urbach [25] tail. The width of the Urbach tail is characteristic of the amount of disorder, whether that disorder be intrinsic (as in amorphous films), or the result of grain boundaries, atomic defects, or other sources. In colloidal QD arrays, the non-stoichiometric, multifaceted surfaces which are imperfectly passivated are a likely source of disorder and trap states, and are included with the other sources in determining the width of the Urbach tail. In a-Si:H, for example, the Urbach edges stem from Si-Si bond angle and length disorder [26]. In PbSe QDs, calculations indicated the presence of significantly more bond angle disorder than in bulk PbSe [27], thus Urbach energies similar to those of amorphous materials are expected.

Cody *et al*. found a semi-empirical equation to describe Urbach tail distributions [28]

$$E_U(T,X) = K\{< U^2 >_T + < U^2 >_X\}, \quad (1)$$

where, $<U^2>_T$ is related to the thermal average of atomic displacements. In crystalline semiconductors, $<U^2>_T$ is the only contribution to the Urbach energy. In disordered materials, $<U^2>_X$ becomes prominent as it describes other, non-thermal, sources of disorder. Even perfectly crystalline semiconductors have an exponential DOS extending into the band gap; however with steep decay, ~5-10 meV (smaller characteristic slopes indicate sharper band tails). As the structure becomes more disordered due to grain boundaries, point defects, etc., the tail broadens significantly. Reported E_U for various single crystal,

amorphous, and nanocrystalline material systems are compared in Table 1 illustrating that the more disorder the system exhibits, the higher E_U.

TABLE I. Characteristic Urbach Energy slopes for various semiconductor systems

Material		E_g (eV)	E_U (meV) [Ref]
Si (single crystal)		1.12	8.5[29]
$Cu(In_{1-x}Ga_x)Se_2$ (poly crys.)		1.0-1.8	15-26[30, 31]
PbS (NC arrays, this work)		0.76-1.96	13.5-19
a-Si:H		1.8	45 (E_V)[32]
Anatase TiO_2	Single crystal	3.4	40[33]
	Porous	3.4	50[34]
	4-8 nm NC	3.4	78[34]
CdS (NC)		2.4	90[35]
CdTe (NC)		1.8	97[36]
Pentacene (single crystal)		2.25	109[37]

Early work on E_U in QD arrays found evidence of broad Urbach tails in nanostructured CdSe [38] and ZnSe [39]. Optical absorption of colloidal CdTe QD films show a broad band tail (97 meV), which reduces (to 30 meV) when the film is sintered to form larger grains [36]. However, optical absorption does not necessarily correlate with carrier transport. Recent work on the *local* transport characteristics of PbS QD arrays with temperature-dependent photoluminescence [40] includes thermal emission from an exponential DOS extending into the gap, consistent with transport models. The characteristic slope of the decay ranged from 15 to 42 meV, increased with increasing ligand length and decreased with QD size. That investigation provides strong evidence for the influence of the Urbach tail on carrier transport characteristics. However, PL measurements probe the microscopic carrier dynamics as the carriers recombine within fairly short distances.

Here, external current detection extends our previous work to macroscopic arrays of QDs, as found in optoelectronic devices. PbS QDs made using hot-injection colloidal synthesis [41] were deposited by either dipcoating from hexane with 0.005 M thiol solutions in acetonitrile [42] or dropcasting and soaking in diluted hydrazine [15]. Heterojunction diodes of the structure ITO/ZnO/PbS/Au were examined with QD band gaps between 1.26 eV (980 nm) and 1.96 eV (633 nm) depending on the diameter of the QDs [43]. The PbS QD layers were ~400 nm thick. A Schottky-barrier device [1], with the reversed device polarity: ITO/PbS/Ca-Al was investigated to rule out contributions from the ZnO-layer and interface. In addition, several low-band gap PbS devices (~1630 nm, 0.76 eV) were examined in a DC-biased planar photodetector geometry with different capping ligands: EDT, 1,4-butanedithiol (BDT) and 1,5-pentanedithiol (PDT). In these devices the Au electrodes were 2 mm long with 25-μm channel spacing. In each experiment, monochromatic light slightly above the band gap (low absorption

coefficient) was used so that charges were generated uniformly throughout the sample. For the photodetector devices, a 1310 nm laser diode was used so as to avoid generating charges in the Si substrates. These samples were only ~50 nm thick, thus charge generation can be assumed to be fairly uniform throughout the film.

The photocarrier transport kinetics were characterized using intensity-modulated photocurrent spectroscopy (IMPS). The use of a lock-in amplifier to analyze the magnitude and phase shift of the AC photoresponse of a sample as a way to determine the sub-band gap DOS was first introduced by Oheda *et al*. [44] and later refined by Brüggeman *et al*. [45] and Hattori *et al*. [46] The experiment is illustrated schematically in Fig. 1A. Briefly, the temperature and frequency at which the experiment is carried out define an emission energy $E_\omega = k_B T \ln(v_0/2\pi f)$ (v_0 is the thermal emission prefactor) from the band edge where the peak of the AC response of the sample originates. A trap state within the band gap will give different relative contributions to the in- and out-of-phase AC response. For example, carriers that fall into trap states close to the band edge will be re-emitted quickly, contributing to the in-phase response. On the other hand, carriers persist longer in trap states that are deeper in the gap, inducing a phase shift. By examining the number of AC photocarriers that are collected and the phase angle between the frequency of the incident light and the output photocurrent, the structure of the DOS near the band edge can be determined. The derivation described by Brüggeman, results in equation 2,

$$N_t(E_\omega) = \frac{2}{\pi k_B T \nu \sigma}\left\{\frac{f e \mu E A}{I(\omega)}\sin(\phi) - \omega\right\} \tag{2}$$

in which, v is the thermal velocity, σ is the carrier capture cross-section, f is the AC generation rate, e is the fundamental charge unit, μ is the mobility, E is the electric field across the film, and A is the sample area. Φ and $I(\omega)$ ($\omega = 2\pi f$) are the observed phase shift and AC photocurrent, respectively.

Equation 2 directly estimates the DOS as a function of energy from the magnitude and phase shift of the photocurrent. This equation is convenient because of its simplicity and insensitivity to noise, but has a limited energy resolution of k_BT. Therefore, if the $E_U < k_BT$, the slope will appear equal to k_BT. The frequency term ω within the braces is negligible, and if information such as the carrier capture cross-section or thermal velocity are unknown (as is the situation with the PbS QD arrays studied here), then the general shape of the DOS can be found from $\sin(\varphi)/I(\omega)$.

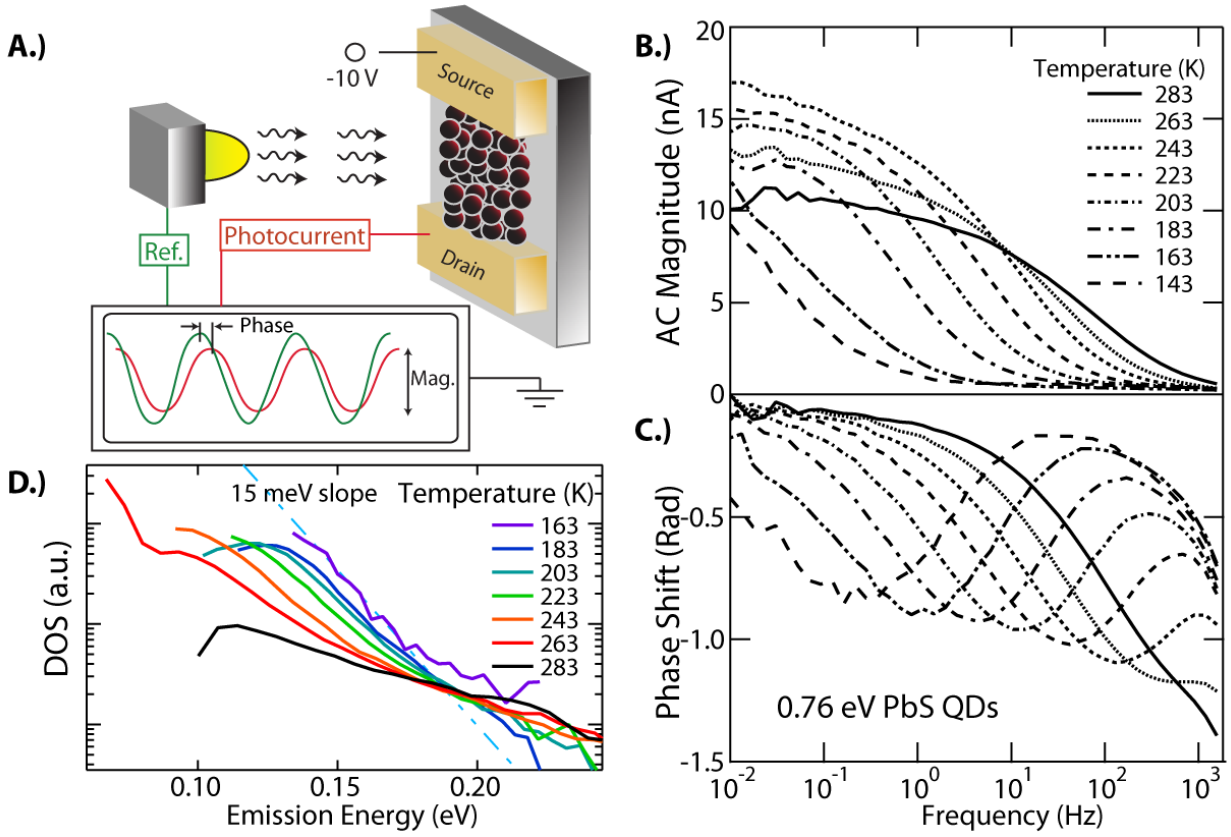

FIG 1. (a) Schematic of IMPS measurement where a film of PbS QDs is contacted with coplanar electrodes of Au prepatterned on a SiO_2/Si substrate. The film is held at 10V DC bias between the drain and source. Pulsed light is incident on the photoconductive PbS QD film, which is collected by a lock in amplifier. The AC magnitude and phase of the current are plotted *vs.* various pulse frequencies of the light source and film temperature. AC photocurrent response of the magnitude (b) and phase shift (c) of a coplanar film composed of PbS QDs (1633 nm 1s exciton peak) with EDT capping ligands. Photoexcited carriers undergo multiple trapping events in the localized states in the band tail, which induces a phase shift with respect to the incident AC modulation. (d) Hattori analysis of the density of tail states for the raw data shown in (b-c) with a fit to the lowest temperature data line indicating a E_U of 15 meV.

As an alternative to Eq. 2, the DOS derived by Hattori *et al.* is less tolerant to noise, but has an increased energy resolution of $k_BT/2$.

$$N(E_\omega) \propto \frac{\partial\left(\frac{cos\phi}{I(\omega)}\right)}{\partial \ln(\omega)} \tag{3}$$

We employ both analysis formalisms and reach the same conclusion. The temperature-dependent IMPS measurements were conducted on a cold stage in nitrogen atmosphere with optical excitation through a quartz window. The amplitude of the AC perturbation was kept below 10% of the DC bias light to ensure that the sample response was linear with the magnitude of the AC signal. There was no difference in the IMPS derived DOS as the amplitude of the AC perturbation was changed from 5% to 20% of the DC bias

light intensity. As the DC bias light intensity was increased, charge transport in the films became faster, as referenced by a shift in the minimum in the phase shift (Fig 1C) to higher frequencies. We note that the DC photocurrent in the solar cell devices was nonlinear with light intensity; however this was most likely due to the decay of photocurrent after the intensity was increased. Measurements taken immediately after the intensity change were much more linear with intensity, suggesting some charge re-arrangement within the sample in agreement with literature [22]. Mott-Schottky carrier densities, derived from DC capacitance-voltage measurements, were near $2x10^{16}$ cm^{-3}, similar to previous reports [1].

Figures 1B-C show the in-phase and out-of-phase current response of representative samples as a function of light modulation frequency and sample temperature. Representative data are shown (fig. 1 (B and C) from the EDT-treated PbS QDs with 1630 nm first exciton peak, in coplanar geometry, with 10 V applied between the source and drain contacts, leading to a 4 kV/cm electric field and using 1310 nm monochromatic light. The peak observed in the phase moved towards lower frequencies at lower temperature, indicative of a thermally-activated process. The activation energy of 250 meV and a thermal emission prefactor of near $10^{5.7}$ s^{-1} are obtained from an Arrhenius plot. These are likely the characteristics of a discrete defect located within the band gap of the PbS QD array. Such low thermal emission prefactors have been measured in other materials, amorphous Si for example[47]. Determining the thermal emission prefactor allows us to estimate the energy scale for subsequent measurements and analysis, as will follow.

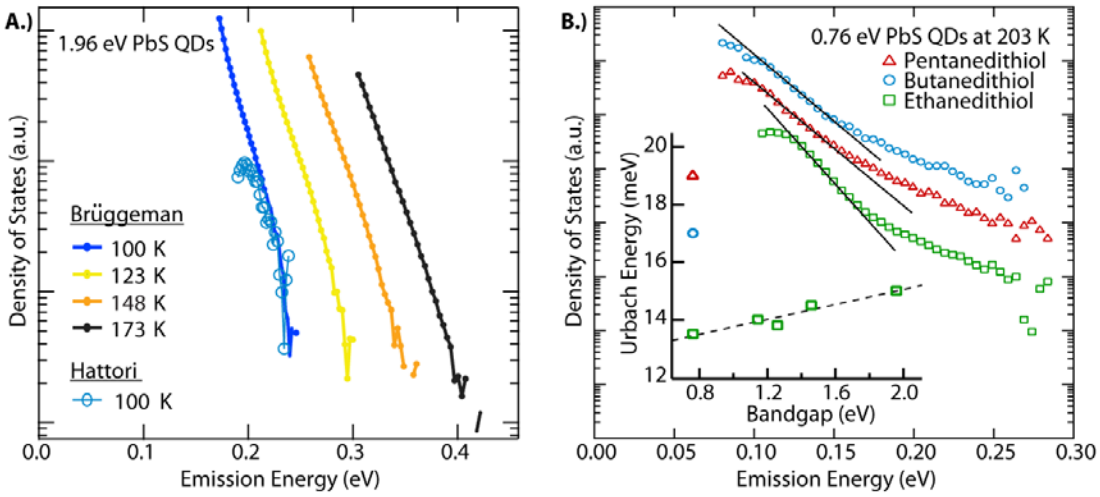

FIG 2 (a) **Bruggeman (Eq. 2) *vs.* Hattori (Eq. 3) analysis of the AC photocurrent response of a ZnO/PbS PV device consisting of 1.96 eV PbS QDs (1s exciton at 633 nm) with EDT capping ligands.** (b) **Various length alkyl-chain capping groups (ethane-, butane-, and pentane-dithiol) on the same sample of PbS QD (1630 nm, shown here) result in broader Urbach edges. (inset) Summary of the distribution of Urbach energies *vs.* band gap of PbS QD array films and for different ligand lengths.**

Figure 2A shows the IMPS data for a solar cell made from 1.96 eV PbS QDs. At low temperature (100 K) both the Brüggeman and Hattori analyses show the same slope, verifying that the analysis is not limited by the temperature of the measurement. Additionally, the slope of the exponential is temperature independent for 100 K, 123 K and 148 K. At 173 K, broadening is apparent in the linear analysis as $k_BT \sim E_U$. The similarity of the E_U is remarkable for samples with such disparate band gap energies (0.76 eV vs 1.96 eV) and for two different device geometries. An increase in E_U with decreasing QD-size (inset of Fig. 2B), is consistent with the idea that as the QD-size decreases, the distribution of localized trap states near the band edge will become broader but the magnitude of the increase is less then observed in temperature-dependent PL measurements[40]. A viable explanation is that PL measurements are sensitive to the exponential band tails of both the conduction and valence bands, which could lead to broader distributions. IMPS, on the other hand, reflects only one of the band tails, whichever has the higher $\mu/(\sigma N(E_\omega))$ value[48]. If we assume that PbS QD arrays behave similarly to PbSe QD arrays, then we can assign a hole mobility that is roughly an order of magnitude lower than the electron mobility[22]. If the trap densities near E_V and E_C are nearly equal, then the transport kinetics of the electrons dominate the IMPS measurement, and it is the conduction band tail that we are measuring. However, if the trap densities near the conduction band are much higher than near the valence band edge, we would expect to measure the valence band tail. All of QD arrays in both the solar cell and coplanar geometries that we studied show similar values of E_U, thus we believe we are measuring the same band tail in all of the devices.

In spite of not being able to definitively identify which carrier is dominating the transport dynamics, it is very surprising to identify such a steep exponential band tail in such a highly disordered system. We note that multiple samples of each QD size were examined, and all exhibited similar results to those presented here. E_U does not increase significantly even when the QDs used to make the films are intentionally very polydisperse. The group of EDT-treated PbS QD samples included a film made from intentionally polydisperse QD-sizes. Even this array, with a 1.14 eV first exciton "peak" and a 200 nm (176 meV) FWHM distribution, showed a 14 meV Urbach edge, suggesting that randomly dispersed larger QDs in the array are not responsible for the Urbach edge. This finding agrees with other results on intentionally polydisperse films, where there was very little change in transport characteristics or solar cell performance parameters until surprisingly high levels of size dispersion [22, 49]. In QD films, carriers may be conducted through $1S_e$ and $1S_h$ states and band tail states on the low energy side of the distribution, well below the average $1S_e$-$1S_h$ levels derived from optical absorption. This renders the energetic width and center of the core exciton state distribution less important.

The influence of capping ligand length on E_U was also explored (Fig 2B). Alkyl ethane-, butane-, and pentane-dithiol ligands, with two, four, and five carbon atoms, respectively, were used to couple the 1630 nm PbS QDs into arrays. This strategy has been used [22] to vary the QD separation within the array. While all samples showed the same general IMPS behavior, the exponential band tail was noticeably broader for longer-chain ligands (inset of Fig. 2B) and is consistent with previous temperature dependent PL results [40], and those of Liu *et al*.[22] who found that increasing inter-dot ligand length leads to decreased mobilities.

Even in very well studied systems such as bulk Si, the microscopic origins of the band tails are not entirely clear. However, it is certain that fluctuations in potential, such as those arising from localized charges, are likely to widen the band tail. Although bulk defects or impurities are unlikely in QDs,

surfaces are known to harbor trap states due to nonstoichiometry and imperfect passivation of dangling bonds. They also have the added complication of an organic capping ligand. The dependence of the E_U on capping ligand suggests that the ligands have an influence on E_U, however are likely not the source of the traps themselves. Instead, perhaps the different ligands passivate the surfaces more or less efficiently, which can change the amount of trapped charge on the surface of the QDs which in turn changes the potential fluctuations a carrier sees as it moves through the sample. There are several potential causes of the larger E_U as ligand length increases; it could be due to decreased coupling between adjacent QDs, leading to localized rather than extended states, or to a larger dispersion in coupling because of a larger degree of conformational flexibility in the longer-chain ligands, or it might simply reflect that the majority of the disorder influencing charge transport originates at or near the QD-surface.

These samples also showed evidence for a separate deeper level sub-band gap defect state in the shoulder feature extending to high emission energies, also shown in Fig 1D. In all three samples, this state had an activation energy near 0.2 eV. We did not observe similar features in the wider-gap QD arrays, suggesting that either 1) the state was not present or 2) that it cannot be detected with the current measurement capabilities. Such a deeper state could, however, be responsible for the low V_{OC}'s seen in PbS QD photovoltaic devices[10]. If this trap state could be passivated or neutralized, then the V_{OC} would only be limited by the tail states and exceptionally high V_{OC}'s could be attained in PbS QD photovoltaic devices due to the sharp band tails measured here.

In conclusion, small perturbation AC measurements of photocarrier transport in arrays of PbS QDs are consistent with multiple trapping in an exponential band tail. The characteristic slope for EDT-capped PbS QD films is surprisingly small and nearly constant (~14 meV), with only a small dependence on QD size or size dispersion. Broader but still fairly shallow band tails were observed for longer-chain capping groups (BDT and PDT). In spite of the large amount of positional disorder of the QDs, off-stoichiometric surfaces, and organic capping groups, the observed band tails are more analogous to polycrystalline semiconductors such as CIGS or CdTe than very disordered or amorphous semiconductors such as a-Si:H. The disorder in the QD arrays might be expected to result in slow, inefficient carrier transport; instead, the disorder may in fact have very little effect on carrier transport, which will enable the further development of QD array devices which also exploit the favorable properties of the QDs.

Acknowledgements

H.Y.C., J.G., M.C.B, J.C.J., and J.M.L. are funded through the Center for Advanced Solar Photophysics, an Energy Frontier Research Center funded by the U.S. Department of Energy (DOE), Office of Science, Office of Basic Energy Sciences (BES). P.T.E, A.J.F. and J.v.d.L. were funded by the Solar Photochemistry Program of the Division of Chemical Sciences, Geosciences, and Biosciences, Office of Basic Energy Sciences of the U.S. Department of Energy. Funding was provided to the National Renewable Energy Laboratory (NREL) through contract DE-AC36-08GO28308.

References

1. J. M. Luther, M. Law, M. C. Beard, Q. Song, M. O. Reese, R. J. Ellingson and A. J. Nozik, Nano Lett. **8**, 3488 (2008).
2. J.-S. Lee, M. V. Kovalenko, J. Huang, D. S. Chung and D. V. Talapin, Nat Nano **6**, 348 (2011).
3. D. S. Chung, J.-S. Lee, J. Huang, A. Nag, S. Ithurria and D. V. Talapin, Nano Lett. **12**, 1813 (2012).

4. L. Sun, J. J. Choi, D. Stachnik, A. C. Bartnik, B.-R. Hyun, G. G. Malliaras, T. Hanrath and F. W. Wise, Nat Nano **7**, 369 (2012).
5. M. C. Beard, A. G. Midgett, M. C. Hanna, J. M. Luther, B. K. Hughes and A. J. Nozik, Nano Lett. **10**, 3019 (2010).
6. O. E. Semonin, J. M. Luther, S. Choi, H.-Y. Chen, J. Gao, A. J. Nozik and M. C. Beard, Science **334**, 1530 (2011).
7. A. H. Ip, S. M. Thon, S. Hoogland, O. Voznyy, D. Zhitomirsky, R. Debnath, L. Levina, L. R. Rollny, G. H. Carey, A. Fischer, K. W. Kemp, I. J. Kramer, Z. Ning, A. J. Labelle, K. W. Chou, A. Amassian and E. H. Sargent, Nat Nano **7**, 577 (2012).
8. E. H. Sargent, Nature Photonics **6**, 133 (2012).
9. A. G. Pattantyus-Abraham, I. J. Kramer, A. R. Barkhouse, X. Wang, G. Konstantatos, R. Debnath, L. Levina, I. Raabe, M. K. Nazeeruddin, M. Graetzel and E. H. Sargent, ACS Nano **4**, 3374 (2010).
10. P. Guyot-Sionnest, J. Phys. Chem. Lett. **3**, 1169 (2012).
11. H. E. Romero and M. Drndic, Phys. Rev. Lett. **95**, 156801 (2005).
12. T. S. Mentzel, V. J. Porter, S. Geyer, K. MacLean, M. G. Bawendi and M. A. Kastner, Phys. Rev. B **77**, 075316 (2008).
13. E. Talgorn, Y. Gao, M. Aerts, L. T. Kunneman, J. M. Schins, T. J. Savenije, A. van HuisMarijn, S. J. van der ZantHerre, A. J. Houtepen and D. A. SiebbelesLaurens, Nat Nano **6**, 733 (2011).
14. P. Nagpal and V. I. Klimov, Nat Commun **2**, 486 (2011).
15. D. V. Talapin and C. B. Murray, Science **310**, 86 (2005).
16. J. J. Choi, C. R. Bealing, K. Bian, K. J. Hughes, W. Zhang, D.-M. Smilgies, R. G. Hennig, J. R. Engstrom and T. Hanrath, J. Am. Chem. Soc. **133**, 3131 (2011).
17. M. I. Bodnarchuk, E. V. Shevchenko and D. V. Talapin, J. Am. Chem. Soc. **133**, 20837 (2011).
18. M. Law, J. M. Luther, Q. Song, B. K. Hughes, C. L. Perkins and A. J. Nozik, J. Am. Chem. Soc. **130**, 5974 (2008).
19. B. K. Hughes, D. A. Ruddy, J. L. Blackburn, D. K. Smith, M. R. Bergren, A. J. Nozik, J. C. Johnson and M. C. Beard, ACS Nano **6**, 5498 (2012).
20. L. Zhang, Q. Song and S. B. Zhang, Phys. Rev. Lett. **104**, 116101 (2010).
21. F. Xu, X. Ma, C. R. Haughn, J. Benavides, M. F. Doty and S. G. Cloutier, ACS Nano **5**, 9950 (2011).
22. Y. Liu, M. Gibbs, J. Puthussery, S. Gaik, R. Ihly, H. W. Hillhouse and M. Law, Nano Lett. **10**, 1960 (2010).
23. T. A. Burr, A. A. Seraphin, E. Werwa and K. D. Kolenbrander, Phys. Rev. B **56**, 4818 (1997).
24. I. Moreels, B. Fritzinger, J. C. Martins and Z. Hens, J. Am. Chem. Soc. **130**, 15081 (2008).
25. F. Urbach, Physical Review **92**, 1324 (1953).
26. Y. Pan, F. Inam, M. Zhang and D. A. Drabold, Phys. Rev. Lett. **100**, 206403 (2008).
27. A. Franceschetti, Phys. Rev. B **78**, 075418 (2008).
28. G. D. Cody, T. Tiedje, B. Abeles, T. D. Moustakas, B. Brooks and Y. Goldstein, Journal de Physique **10**, 301 (1981).
29. C. H. Grein and S. John, Phys. Rev. B **39**, 1140 (1989).
30. P. T. Erslev, J. Lee, G. M. Hanket, W. N. Shafarman and J. D. Cohen, Thin Solid Films **519**, 7296 (2011).
31. J. T. Heath, J. D. Cohen, W. N. Shafarman, D. X. Liao and A. A. Rockett, Appl. Phys. Lett. **80**, 4540 (2002).
32. R. A. Street, *Hydrogenated amorphous silicon*. (Cambridge University Press, New York, 1991).
33. H. Tang, F. Lévy, H. Berger and P. E. Schmid, Phys. Rev. B **52**, 7771 (1995).
34. V. Duzhko, V. Y. Timoshenko, F. Koch and T. Dittrich, Phys. Rev. B **64**, 075204 (2001).
35. A. Podborska, B. Gaweł, Ł. Pietrzak, I. B. Szymańska, J. K. Jeszka, W. Łasocha and K. Szaciłowski, J. Phys. Chem. C **113**, 6774 (2009).

36. A. Bezryadina, C. France, R. Graham, L. Yang, S. A. Carter and G. B. Alers, Appl. Phys. Lett. **100**, 013508 (2012).
37. D. V. Lang, X. Chi, T. Siegrist, A. M. Sergent and A. P. Ramirez, Phys. Rev. Lett. **93**, 086802 (2004).
38. B. Pejova and B. Abay, J. Phys. Chem. C **115**, 23241 (2011).
39. B. Pejova, B. Abay and I. Bineva, J. Phys. Chem. C **114**, 15280 (2010).
40. J. Gao and J. C. Johnson, ACS Nano **6**, 3292 (2012).
41. C. B. Murray, C. R. Kagan and M. G. Bawendi, Annu. Rev. Mater. Sci. **30**, 545 (2000).
42. J. M. Luther, M. Law, Q. Song, C. L. Perkins, M. C. Beard and A. J. Nozik, ACS Nano **2**, 271 (2008).
43. J. Gao, J. M. Luther, O. E. Semonin, R. J. Ellingson, A. J. Nozik and M. C. Beard, Nano Lett. **11**, 1002 (2011).
44. H. Oheda, J. Appl. Phys. **52**, 6693 (1981).
45. R. Bruggemann, C. Main, J. Berkin and S. Reynolds, Phil. Mag. B **62**, 29 (1990).
46. K. Hattori, Y. Niwano, H. Okamoto and Y. Hamakawa, J. Non-Cryst. Solids **137-138**, 363 (1991).
47. R. S. Crandall, Phys. Rev. B **36**, 2645 (1987).
48. C. Longeaud and J. P. Kleider, Phys. Rev. B **45**, 11672 (1992).
49. D. Zhitomirsky, I. J. Kramer, A. J. Labelle, A. Fischer, R. Debnath, J. Pan, O. M. Bakr and E. H. Sargent, Nano Lett. **12**, 1007 (2012).